Analytica Chimica Acta 687 (2011) 193–200

Contents lists available at ScienceDirect

Analytica Chimica Acta

journal homepage: www.elsevier.com/locate/aca

Chitosan-*g*-poly(acrylic acid) hydrogel with crosslinked polymeric networks for Ni^{2+} recovery

Yian Zheng[a,b], Dajian Huang[a,b], Aiqin Wang[a,*]

[a] Center of Eco-materials and Green Chemistry, Lanzhou Institute of Chemical Physics, Chinese Academy of Sciences, Tianshui Middle Road 18#, Lanzhou 730000, Gansu, China
[b] Graduate University of the Chinese Academy of Sciences, Beijing 100049, China

ARTICLE INFO

Article history:
Received 2 November 2010
Received in revised form
15 December 2010
Accepted 16 December 2010
Available online 23 December 2010

Keywords:
Hydrogel
Adsorption
Nickel
Recovery
Mechanism

ABSTRACT

In this study, chitosan-*g*-poly(acrylic acid) (CTS-*g*-PAA) hydrogel with crosslinked polymeric networks was prepared from an aqueous dispersion polymerization and then used as the adsorbent to recover a valuable metal, Ni^{2+}. The adsorption capacity of CTS-*g*-PAA for Ni^{2+} was evaluated and the adsorption kinetics was investigated using Voigt-based model and pseudo-second-order model. In addition, the effects of pH values and coexisting heavy metal ions such as Cu^{2+} and Pb^{2+} on the adsorption capacity were studied. The results indicate that the as-prepared adsorbent has faster adsorption rate and higher adsorption capacity for Ni^{2+} recovery, with the maximum adsorption capacity of 161.80 mg g^{-1}. In a wide pH range of 3–7, the adsorption capacity keeps almost the same, and even under competitive conditions, the adsorption capacity of CTS-*g*-PAA for Ni^{2+} is observed to be as high as 54.47 mg g^{-1}. Finally, the adsorption performance of CTS-*g*-PAA for Ni^{2+} in real water sample and the reusability of the as-prepared adsorbent were evaluated, and also the controlled adsorption mechanism was proposed.

1. Introduction

Recently, the demand for nickel in the world market is progressively growing, while primary resources are being depleted. Nickel is a valuable metal used for the production of austenitic stainless steel, super alloys, non-ferrous alloys, steel alloys, rechargeable batteries, and catalysts [1]. No matter how valuable it is, nickel is observed to produce a general toxic effect on human organism and be hazardous to the ecosystem. The inhalation of nickel and its compounds can lead to serious problems, such as nasopharynx, lung and dermatological diseases, and malignant tumors [2]. From the viewpoints of economical and environmental impacts, the guarantee for recovery and enrichment of nickel is rather high [3–5].

The traditional methods used in industry for recovering and separating nickel from solution include co-precipitation, solvent extraction, ion-exchange, reverse osmosis, electrodialysis, membrane separation, etc. [5–7]. These methods have respective limitations: difficult to filter, consuming large amounts of organic solvent, high operation cost, low metal ions retention capacity, and long separation time. As an alternative, adsorption or solid-phase extraction is considered to be an effective method for the recovery of valuable Ni^{2+}. It had been reported that Chang et al. used a surface imprinting technique for selective solid-phase extraction of Ni^{2+} [8]. Solid-phase extraction is today the most popular method for pre-concentration and recovery of valuable metals [9–11]. Development of novel solid adsorbents for recovery of these valuable metals from aqueous solution is thus of great importance. An efficient adsorbent material must be a stable and insoluble material having reactive functional groups such as carboxylates that can be used as the chelating sites for capture of some valuable metals.

In recent years, polymer materials have attracted much attention as the adsorbent for recovering or separating metals from impurities [12,13]. Hydrogel is a three-dimensional network of hydrophilic polymers crosslinked by chemical or physical interactions [14,15], and can be prepared with different functional groups such as carboxylic acid, amine, hydroxyl, and sulfonic acid groups. These groups attached onto the polymeric networks can be tailored easily for a specific application [16]. Owing to higher adsorption rate and adsorption capacity, polymer hydrogels can provide many advantages as a novel type, fast-responsive, and high-capacity adsorbent materials for the removal of pollutants from aqueous solution [17–20]. These hydrogels used are generally prepared from free-radical solution polymerization and the resulting product is mainly in the gel-form [21,22], which requires more energy to dry and to smash. In this study, we used chitosan, a biocompatible, biodegradable and nontoxic natural polymer, as the backbone to graft poly(acrylic acid), obtaining a granular hydrogel adsorbent chitosan-*g*-poly(acrylic acid) (CTS-*g*-PAA) by an aqueous dispersion polymerization. CTS-*g*-PAA is a crosslinked polymeric hydrogel that cannot be dissolved in the aqueous solution and organic sol-

* Corresponding author. Tel.: +86 931 4968118; fax: +86 931 8277088.
E-mail address: aqwang@licp.cas.cn (A. Wang).

0003-2670/$ – see front matter © 2010 Elsevier B.V. All rights reserved.
doi:10.1016/j.aca.2010.12.026

vents. Due to the presence of a large amount of functional carboxylic groups, this adsorbent is expected to show higher affinity to Ni^{2+} *via* the chelating interaction between the deprotonated carboxylic groups and Ni^{2+} ions. The attached Ni^{2+} ions can be desorbed from this adsorbent by a small amount of inorganic acid, obtaining thus a high concentration solution of corresponding Ni^{2+} ions by which Ni^{2+} can be enriched and recycled.

2. Experimental

2.1. Instrument and apparatus

FTIR spectra were recorded on a Thermo Nicolet NEXUS^{TM} spectrophotometer using KBr pellets in the range of 400–4000 cm^{-1}. SEM studies were carried out in a JSM-5600LV SEM instrument (JEOL, Ltd.) after coating the sample with gold film using an acceleration voltage of 20 kV. Ni^{2+} content was determined using the dimethylglyoxime spectrophotometric method at the wavelength of 450 nm.

2.2. Materials

Acrylic acid (AA, chemically pure, Shanghai Shanpu Chemical Factory, Shanghai, China) was distilled under reduced pressure before use. Ammonium persulfate (APS, analytical grade, Sinopharm Chemical Reagent Co., Ltd., Shanghai, China), *N*,*N*′-methylene-bisacrylamide (MBA, chemically pure, Shanghai Yuanfan additives plant, Shanghai, China), and chitosan (CTS, deacetylation degree of 0.90, average molecular weight of 3×10^5, Zhejiang Yuhuan Ocean Biology Co., Zhejiang, China) were used as received.

A stock standard Ni^{2+} solution at 1000 mg L^{-1} was prepared by dissolving an appropriate amount of analytical grade sulfate salt in distilled water. The working solutions containing different concentrations of Ni^{2+} were prepared by stepwise dilution of the stock solution. The pH values were adjusted by addition of 0.1 and 1.0 mol L^{-1} NaOH or HCl solution to a designed value (Mettler Toledo FE20 pH-meter). Other reagents used were all analytical grade and all solutions were prepared with distilled water.

2.3. Preparation of CTS-g-PAA

The preparation process of CTS-*g*-PAA is similar to that reported [23] but with a small modification, which is rather simple and more convenient for our purpose: 0.5 g CTS was dissolved in a mixing solution consisted of 3.6 g of AA, 0.1 g of MBA and 45 mL of tap water in a 250 mL four-neck flask equipped with a stirrer, a condenser, a thermometer and a nitrogen line. After removal of oxygen, this solution was heated to 60 °C gradually while 0.1 g of APS was introduced to initiate CTS to generate macro-radicals. The temperature was kept at 70 °C for 3 h to complete the polymerization reaction, and then the resulting granular product was poured into 6.0 mol L^{-1} NaOH solution to pH 7.0 by neutralization. The swollen product was dehydrated with methanol and dried at 70 °C to a constant weight. All samples used for adsorption test had a particle size in the range of 40–80 mesh. The schematic procedure for preparation of CTS-*g*-PAA and the resulting product were shown in Fig. 1. In order to explain the graft reaction, PAA was obtained with the gel-form as a result of the absence of CTS.

2.4. Adsorption experiment

In order to determine the adsorption capacity of CTS-*g*-PAA for Ni^{2+}, as well as the effects of contact time, pH value, and coexisting ions, adsorption experiments were performed by batch equilibrium technique. A typical experiment was performed under 120 rpm with an orbital shaker THZ-98A. The experiments were carried out in a series of 50 mL conical flasks containing 50 mg of hydrogel adsorbent and 25 mL of Ni^{2+} solution. On reaching adsorption equilibrium the adsorbents were separated by direct filtration and the final Ni^{2+} concentrations in the solution were measured.

To evaluate the maximum adsorption capacity, 50 mg of adsorbent was equilibrated with Ni^{2+} solution with different initial concentration (100–800 mg L^{-1}) for 120 min. After the separation, the final Ni^{2+} concentration in the residual solution was determined. For the adsorption kinetic studies, a series of Ni^{2+} solutions of 100 mg L^{-1} or 400 mg L^{-1} were contacted with 50 mg of adsorbent with different contact time (1–90 min), separated and analyzed for residual Ni^{2+} concentration. The effects of pH were studied in the pH range of 2–7 at an initial Ni^{2+} concentration of 100 mg L^{-1} or 400 mg L^{-1} and contact time of 30 min, with the initial pH values being adjusted by adding 0.1 or 1.0 mol L^{-1} NaOH and HCl solutions. In addition, the adsorption capacity of CTS-*g*-PAA for Ni^{2+} was determined under the presence of Cu^{2+} and Pb^{2+} ions and, the adsorption performance of CTS-*g*-PAA for Ni^{2+} in real water sample was evaluated.

2.5. Constants

The adsorption capacity, the adsorption percentage and desorption ratio were calculated according to the following equations:

$$q_e = \frac{(C_0 - C_e)V}{m} \quad (1)$$

$$R_1 = \frac{C_0 - C_e}{C_0} \quad (2)$$

$$R_2 = \frac{q}{q_e} \quad (3)$$

where q_e is the adsorption capacity (mg g^{-1}), q is the desorption capacity (mg g^{-1}), C_0 and C_e are the initial and equilibrium Ni^{2+} concentration (mg L^{-1}), m is the mass of adsorbent used (mg), V is the volume of Ni^{2+} solution (mL), R_1 is the adsorption percentage (%), and R_2 is the desorption ratio (%).

2.6. Desorption and regeneration

Desorption studies were performed by dispersing used adsorbent into different volume of 1.0 mol L^{-1} HCl solution (5, 10, 15, 20, 25, and 30 mL) and agitating at 30 °C for 60 min. Then, the desorbed amount of Ni^{2+} was obtained. The recovered adsorbent was treated with 25 mL of NaOH solution at 0.1 mol L^{-1} to neutralize and recondition the sample for adsorption in succeeding cycles.

2.7. Enrichment and recovery

A 50 mg of adsorbent was contacted with 50 mL of Ni^{2+} solution at 10 mg L^{-1} and agitated at 30 °C for 30 min to reach the adsorption equilibrium. Then the Ni^{2+}-loaded adsorbent was separated and contacted again with another 50 mL of Ni^{2+} solution at 10 mg L^{-1} to reach the adsorption equilibrium. A similar procedure was repeated until the adsorption percentage $R_1 < 95\%$. Then, the Ni^{2+} ions retained on the adsorbent were eluted with 1.0 mol L^{-1} HCl solution to be recovered.

3. Results and discussion

3.1. Characterization of CTS-g-PAA

Chemical modifications are promising ways to obtain various utilizations of polysaccharides, such as CTS in this study. Of possible modifications, graft copolymerization is expected to be quite

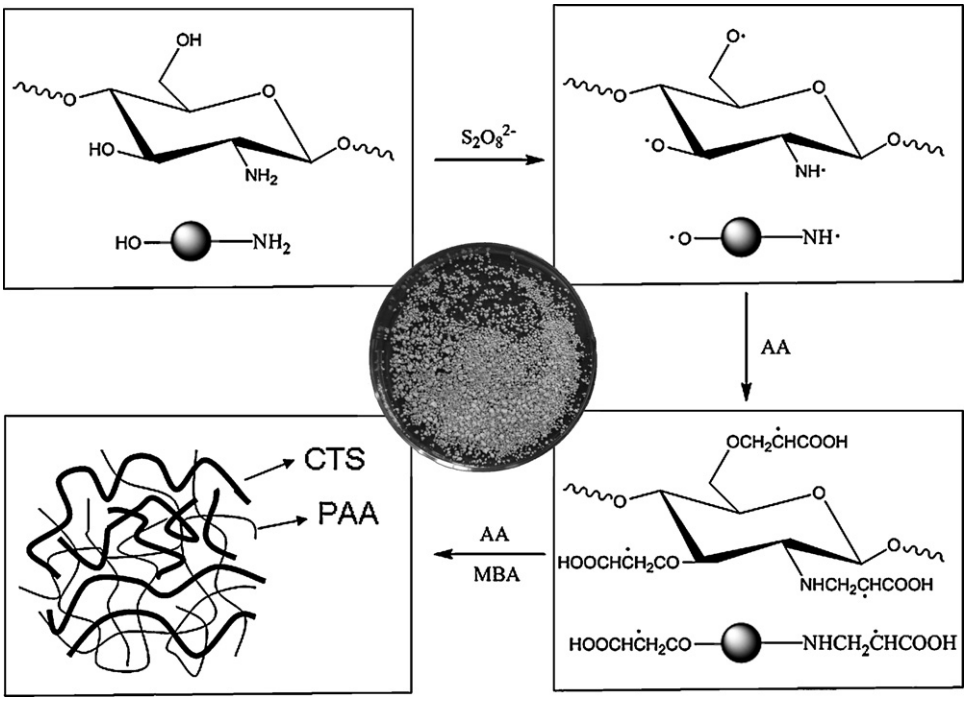

Fig. 1. Schematic preparation of CTS-*g*-PAA and the digital photo of resulting product.

promising for developing sophisticated functions. CTS bears two types of reactive groups that can be grafted. First, the free amino groups on deacetylated units and second, the hydroxyl groups on the C_3 and C_6 carbons on acetylated or deacetylated units [24,25]. The graft copolymerization of CTS with vinyl monomers in water in the presence of APS would give a three-dimensional cross-linked product, and hence enlarge the field of the potential applications of them by choosing various types of side chains. As shown in Fig. 1, a general reaction mechanism for the preparation of CTS-*g*-PAA is proposed as follows: under the heating, the thermal dissociation initiator APS is decomposed to produce a sulfate anion radical. Then, the resulting anion radical abstracts hydrogen atom from $-NH_2$ or –OH groups present in CTS to form macro-radicals. Afterwards, these macro-radicals initiate the grafting reaction of PAA to the backbone of CTS, yielding to a three-dimensional structured graft copolymer.

Fig. 2 shows the FTIR spectra of CTS, PAA and CTS-*g*-PAA. The FTIR spectrum of CTS has strong peak around 3448 cm^{-1} due to the stretching vibration of O–H, the extension vibration of N–H, and inter-molecular hydrogen bonds of the polysaccharide. In addition, the typical absorption bands of CTS at 1654, 1594 and 1328 cm^{-1} are assigned to amide I, amide II and amide III, respectively. In the region of 1000–1200 cm^{-1}, CTS presents a broad absorption band centered at 1091 cm^{-1}, corresponding to stretching of C–O bond of secondary –OH. The band of 1034 cm^{-1} is derived from C–O stretching of primary –OH. The asymmetric stretching of C–O–C appears at 1155 cm^{-1} [26]. After the reaction, these characteristic absorption bands get weaken or masked with other absorption bands, implying

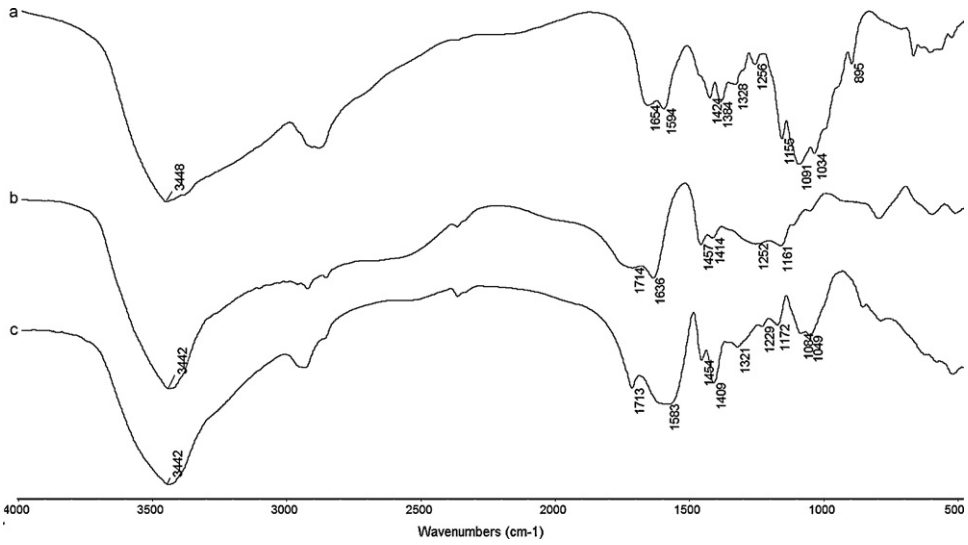

Fig. 2. FTIR spectra of (a) CTS, (b) PAA, and (c) CTS-*g*-PAA.

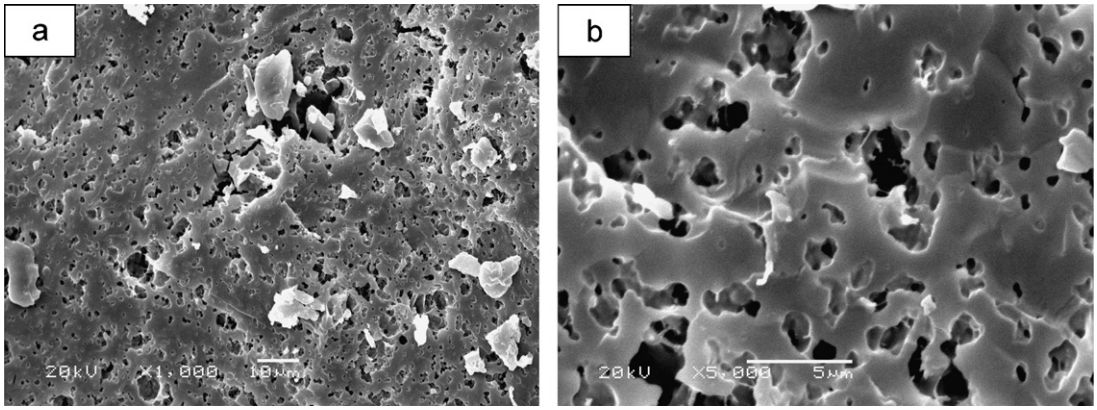

Fig. 3. Scanning electron micrographs of CTS-*g*-PAA: (a) 1000× and (b) 5000×.

that reactive functional groups of CTS, such as $-NH_2$ and –OH, have took part in the copolymerization reaction. The absorption bands in the spectrum of CTS-*g*-PAA at 1713, 1583, 1454 and 1409 cm^{-1} are arisen from PAA and assigned respectively to stretching C=O vibration, asymmetric $-COO^-$ stretching vibration, bending vibration of C–H and symmetric $-COO^-$ stretching vibration. The occurrence of these bands in CTS-*g*-PAA spectrum is a powerful evidence of PAA existence. From above analysis, it is no doubtful that during the reaction, PAA has been grafted on the backbone of CTS.

Fig. 3 shows the micrographs of CTS-*g*-PAA hydrogel. It is clearly observed that the as-prepared adsorbent shows a smooth surface with some micro-pores interspersed on the surface. This surface morphology is beneficial for water permeation, making the Ni^{2+} ions be easily accessible to the reactive functional groups distributed within the polymeric networks, and accordingly, one can speculate that the adsorption equilibrium would be achieved quickly.

3.2. Adsorption capacity

As shown in Fig. 4, the adsorption capacity increases with increasing the initial Ni^{2+} concentration. This is attributed to that an increase in Ni^{2+} concentration can accelerate the diffusion of Ni^{2+} ion into the polymeric networks as a result of an increase in the driving force of concentration gradient. To obtain the maximum adsorption capacity, in this study, the Langmuir model was used to fit these experimental data. The Langmuir isotherm assumes that the adsorption occurs at specific homogeneous sites on the adsorbent and is the most commonly used model for monolayer adsorption process, as represented by the following equation:

$$q_e = \frac{q_m b C_e}{1 + b C_e} \quad (4)$$

where q_e is the equilibrium adsorption capacity of Ni^{2+} on adsorbent (mg g^{-1}), C_e is the equilibrium Ni^{2+} concentration (mg L^{-1}), q_m is the monolayer adsorption capacity of the adsorbent (mg g^{-1}) and b is the Langmuir adsorption constant (L mg^{-1}). By non-linear regression of the experimental data, the calculated q_m, b and correlation coefficient R is found to be 161.80 mg g^{-1}, 0.2905 L mg^{-1} and 0.9936, respectively. It can be seen that the adsorption capacity of CTS-*g*-PAA for Ni^{2+} is rather high.

3.3. Adsorption kinetics

Contact time is an important parameter which reflects the adsorption kinetics of an adsorbent at a given initial adsorbate concentration. The effects of contact time on the adsorption capacity were investigated at an initial Ni^{2+} concentration of 100 mg L^{-1} and 400 mg L^{-1}, as shown in Fig. 5. The adsorption of Ni^{2+} onto CTS-*g*-PAA as a function of contact time illustrated that the adsorption rate was rapid and the adsorption equilibrium could be achieved within 30 min. The as-prepared adsorbent CTS-*g*-PAA has a superhydrophilic polymeric networks and a large amount of reactive

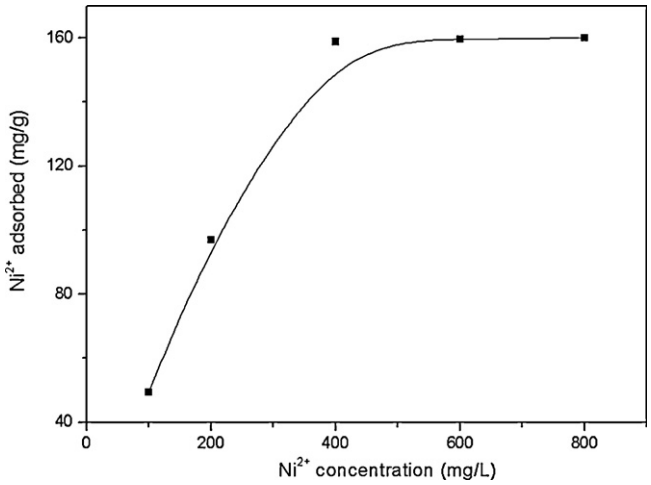

Fig. 4. The change of adsorption capacity as a function of initial Ni^{2+} concentration. Adsorption experiments: C_0, 100–800 mg L^{-1}; t, 120 min; adsorption dose, 50 mg/25 mL; natural pH; 30 °C/120 rpm.

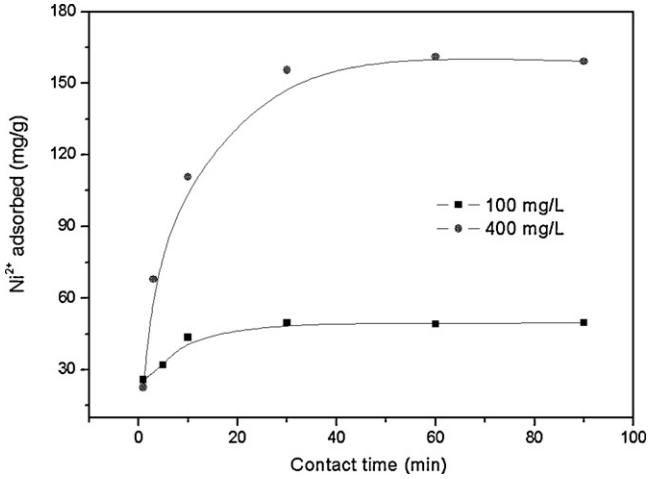

Fig. 5. Variation in the adsorption capacity as a function of contact time. Adsorption experiments: C_0, 100 or 400 mg L^{-1}; t, 1–90 min; adsorption dose, 50 mg/25 mL; natural pH; 30 °C/120 rpm.

Table 1
Estimated adsorption kinetic parameters for Ni^{2+} adsorption.

C_0 (mg L^{-1})	Voigt-based model	Pseudo-second-order model					
	r (min)	q_e (mg g^{-1})	q_e, exp (mg g^{-1})	q_e, cal (mg g^{-1})	k_2 (g mg^{-1} min^{-1})	h (mg g^{-1} min^{-1})	R^2
100	2.03	46.52	49.86	50.76	0.01198	30.86	0.9995
400	6.89	158.1	161.1	169.5	0.001217	34.97	0.9982

functional groups, which is responsible for its fast adsorption for Ni^{2+} ions. This rapid adsorption rate is consistent with the expected results derived from SEM analysis.

In this study, we used the Voigt-based viscoelastic model to characterize the adsorption experimental data, as expressed as follows:

$$q_t = q_e(1 - e^{-t/r}) \quad (5)$$

where q_t is the adsorption capacity at any moment (mg g^{-1}), q_e is the equilibrium adsorption capacity (mg g^{-1}), t is the adsorption time (min), and r is the adsorption rate parameter (time required to reach 0.63 of equilibrium adsorption capacity) (min). By fitting into the above equation (Table 1), the adsorption rate parameter r was calculated to be 2.03 and 6.89 min, respectively, while the equilibrium adsorption capacity was found to be 46.52 and 158.1 mg g^{-1}, respectively, when the initial Ni^{2+} concentration was fixed at 100 mg L^{-1} and 400 mg L^{-1}, respectively. These data give an indication that the adsorption of Ni^{2+} onto the as-prepared adsorbent is a rapid adsorption process, though some differences in the adsorption rate have been observed at different initial Ni^{2+} concentration.

In order to understand better the adsorption process, the pseudo-second-order equation was also applied to test the adsorption experimental data:

$$\frac{t}{q_t} = \frac{1}{k_2 q_e^2} + \frac{t}{q_e} \quad (6)$$

where q_e and q_t are the amounts of Ni^{2+} adsorbed (mg g^{-1}) at equilibrium and at time t, respectively. k_2 is the rate constant of pseudo-second-order adsorption (g mg^{-1} min^{-1}), which can be determined from the straight-line plot of t/q_t against t. The initial adsorption rate h (mg g^{-1} min^{-1}) can be obtained using the equation of $h = k_2 q_e^2$. These parameters and correlation coefficient R^2 were calculated and listed in Table 1. It is observed that the correlation coefficient R^2 for pseudo-second-order kinetic model is above 0.99, indicating that the pseudo-second-order kinetic model can describe well the adsorption experimental data. In addition, higher initial Ni^{2+} concentration can provide the higher driving force, leading thus a higher initial adsorption rate. From the conclusions drawn from studies on adsorption capacity and adsorption kinetics, it is convinced that CTS-*g*-PAA has high adsorption capacity and fast adsorption rate for Ni^{2+} recovery, which can be further clearly confirmed from a comparative study, as listed in Table 2.

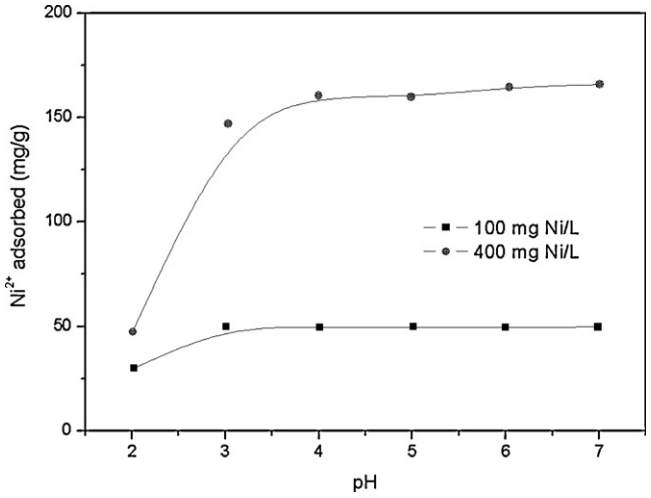

Fig. 6. Effects of pH on the Ni^{2+} adsorption capacity. Adsorption experiments: C_0, 100 or 400 mg L^{-1}; t, 30 min; adsorption dose, 50 mg/25 mL; pH, 2–7; 30 °C/120 rpm.

3.4. pH-dependence

During the adsorption process, the pH value is generally the key parameter, because it controls not only the surface charge of an adsorbent, but also the chemical nature of metallic cations. The effects of pH on the adsorption capacity are shown in Fig. 6. CTS-*g*-PAA, used in this study, is an ionic polymer matrix. At lower pH value, it is observed that the adsorption capacity decreases appreciably. This fact is ascribed to that the reactive functional groups within the polymeric networks are shown as protonated form, which can hinder the interaction between the adsorbent and cation. In addition, non-ionic bonding mechanism (e.g. hydrogen bonding) among carboxylic groups occurs at lower pH value, which is also responsible for lower metal ion adsorption capacity. With an increase in pH values, the adsorption capacity increases since the dissociation of carboxylic groups is favored at higher pH values, by which ionic bonds form between polymer backbone and metal ions. Here, it is worthy pointing out that the adsorption capacity of CTS-*g*-PAA to Ni^{2+} keeps almost constant in a wide pH range of 3–7. For other adsorbents reported, the adsorption capacity is generally pH-dependent [27,29,32]. Beyond pH 7, a precipitate would be formed immediately. Based on these discussions, the pH of Ni^{2+} solution should be adjusted in the range between 3 and 7 during the adsorption process.

Table 2
Comparison of the adsorption capacities of Ni^{2+} onto different adsorbents.

Adsorbents	Maximum adsorption capacity (mg g^{-1})	Equilibrium time (min)	Reference
Bentonite	4.32	–	[27]
Sodium montmorillonite	10.65	230	[28]
Clinoptilolite	15.55	500–1000	[29]
Polyethyleneimine-attached poly(p-chloromethylstyrene) beads	78.2	150	[30]
Chitosan	86.51	1440	[31]
CTS-*g*-PAA	161.8	30	This study

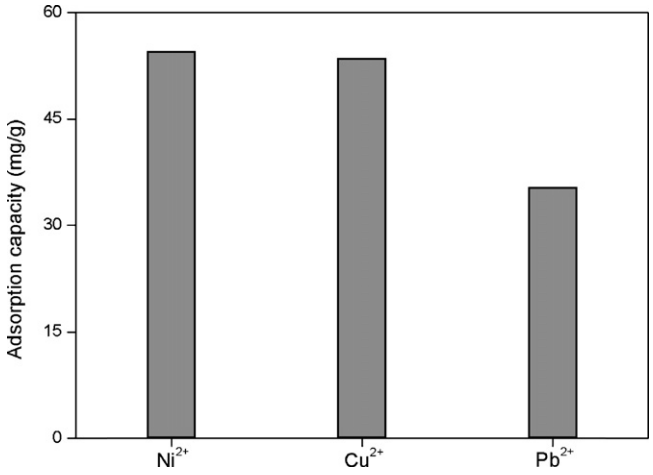

Fig. 7. Adsorption capacity of CTS-*g*-PAA for Ni^{2+} in the presence of Cu^{2+} and Pb^{2+}. Adsorption experiments: C_0, 100 mg L^{-1} for each metal ion; *t*, 60 min; adsorption dose, 50 mg/25 mL; natural pH; 30 °C/120 rpm.

Table 3
Determination results of CTS-*g*-PAA for Ni^{2+} recovery in real water sample.

Ni^{2+} concentration (mg L^{-1})	Adsorption capacity (mg g^{-1})	Adsorption percentage (%)
16.19	7.975	98.72
52.29	25.88	99.17
101.1	50.37	99.44

3.5. Competitive adsorption

Some other heavy metals such as Cu^{2+} and Pb^{2+} may coexist with Ni^{2+} in industrial wastewater, and thus it is important to investigate the adsorption capacities of CTS-*g*-PAA for Ni^{2+} in the presence of these coexisting ions. Under competitive conditions, the adsorption capacity of CTS-*g*-PAA for Ni^{2+}, Cu^{2+} and Pb^{2+} is 54.47, 53.47 and 35.33 mg g^{-1}, respectively (Fig. 7). Due to the presence of –COOH and $–COO^-$ groups, the as-prepared adsorbent shows higher affinity towards multivalent metal, but cannot distinguish them from each other. Nevertheless, the higher adsorption capacity of CTS-*g*-PAA for Ni^{2+} proves its potential to recover valuable Ni^{2+} from aqueous solution.

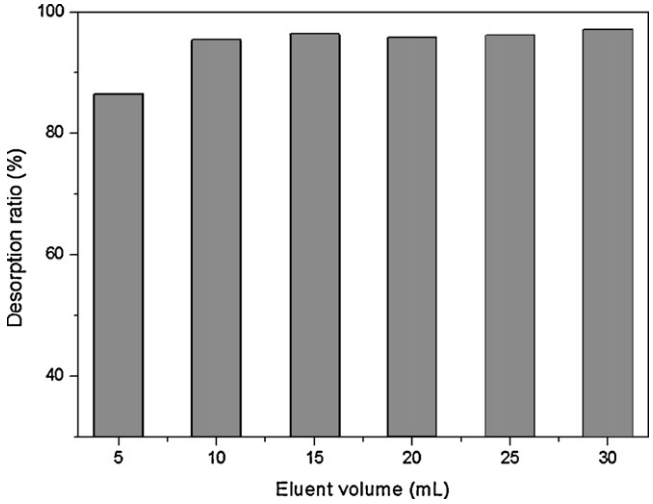

Fig. 8. Desorption ratio as a function of eluent volume. Adsorption experiments: C_0, 400 mg L^{-1}; *t*, 30 min; adsorption dose, 50 mg/25 mL; natural pH; 30 °C/120 rpm. Desorption experiments: 30 °C/120 rpm/60 min.

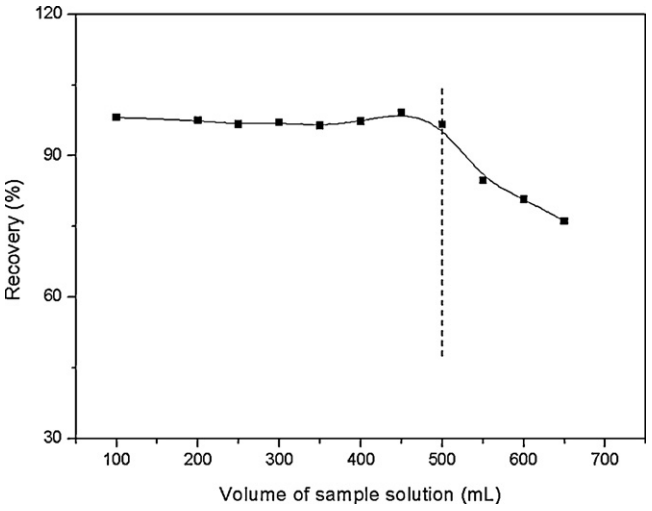

Fig. 9. Effect of sample volume on analytical recovery. Adsorption experiments: C_0, 10 mg L^{-1}; *t*, 30 min; adsorption dose, 50 mg; natural pH; 30 °C/120 rpm.

To assess the efficacy of the as-prepared adsorbent in real water body, a natural water sample collected from Taihu Lake in Jiangsu was used. The basic parameters of water quality were as follows: ammonium-nitrogen (NH_4-N, mg L^{-1}), 0.12; turbidity (NTU), 0.3; COD (mg L^{-1}), 4; pH, 7.68; conductivity (μs cm^{-1}), 597; Cu^{2+} (mg L^{-1}), 1.8×10^{-3}; Pb^{2+} (mg L^{-1}), 1.0×10^{-4}. The concentration of heavy metal ions was so lower that during the experiment, definite three concentrations of Ni^{2+} ion were added into the water sample. The analytical results listed in Table 3 show that in real water sample, the adsorption percentage approximates 99% for different three-level concentrations of Ni^{2+} ions, testifying the good performance of the as-prepared adsorbent for Ni^{2+} recovery.

3.6. Desorption and reusability

Since the protonation of carboxylate groups under stronger acid conditions, the interaction between carboxylate and Ni^{2+} could be easily weaken and subsequently Ni^{2+} ions are released from the adsorbent into the desorbing medium. With 1.0 mol L^{-1} HCl as the eluent, the desorption behavior of Ni^{2+} from CTS-*g*-PAA was investigated using different volume of eluent. The results indicated that the quantitative recoveries (R_2 > 95%) of Ni^{2+} could be obtained

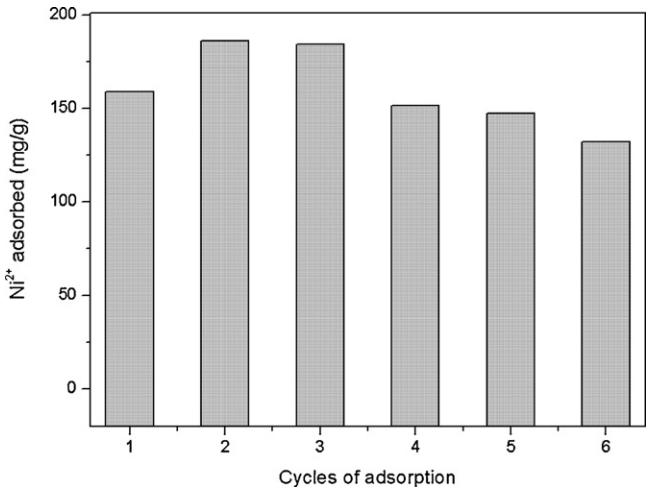

Fig. 10. The amount adsorbed for Ni^{2+} as a function of adsorption–desorption cycle. Adsorption experiments: C_0, 400 mg L^{-1}; *t*, 30 min; adsorption dose, 50 mg/25 mL; natural pH; 30 °C/120 rpm. Desorption experiments: 30 °C/120 rpm/60 min.

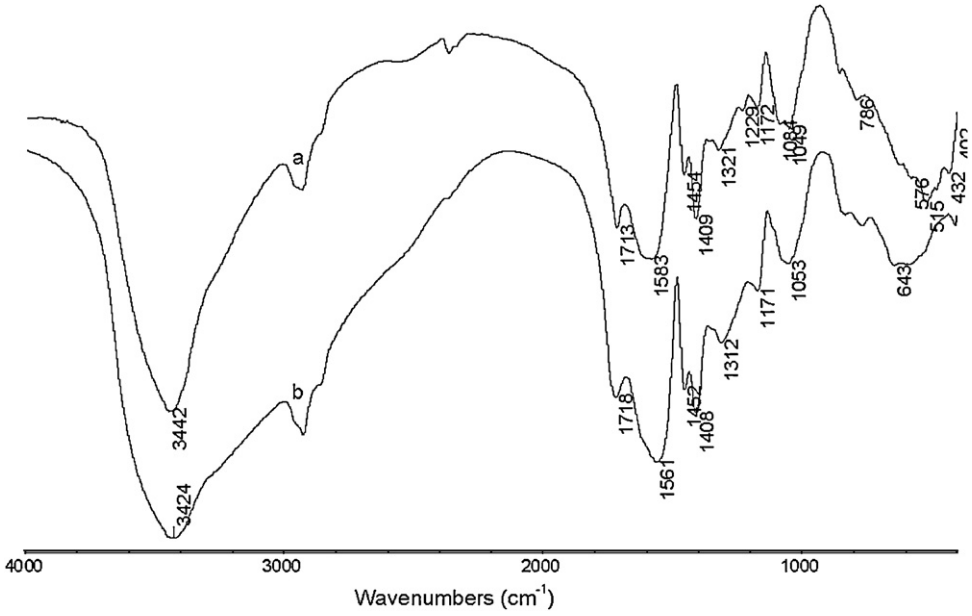

Fig. 11. FTIR spectra of CTS-*g*-PAA before (a) and after (b) adsorption for Ni^{2+}.

using 10 mL of 1.0 mol L^{-1} HCl as the eluent, as shown in Fig. 8. Further increase in the volume of eluent has no obvious contributions to the desorption ratio. Afterwards, the enrichment studies were performed and the results (Fig. 9) suggested that the maximum sample volume treated was up to 500 mL with R_1 of 95% under the conditions of 50 mg of adsorbent and Ni^{2+} solution at 10 mg L^{-1}. The Ni^{2+} ions adsorbed could be desorbed effectively from the as-prepared adsorbent, by which the Ni^{2+} ions would be enriched and recycled.

Reusing ability of an adsorbent during regeneration process is an important parameter. Ni^{2+}-loaded adsorbent was eluted with an acid solution and activated with an alkaline solution as described in the experimental part and used again for Ni^{2+} recovery. As discussions above, the Ni^{2+} ions adsorbed by the sample could be desorbed efficiently (R_2 > 95%). Though the adsorbed Ni^{2+} ions cannot be desorbed completely from the as-prepared adsorbent, some additional adsorption sites can be created during the regeneration process. By a careful comparison of FTIR spectra of CTS-*g*-PAA before and after the regeneration, we have observed that after the regeneration, the stretching vibration of –COOH groups gets weakened and the intensities of asymmetric/symmetric vibration absorption bands of $–COO^-$ groups show a remarkable increase. Compared with –COOH groups, $–COO^-$ groups show higher affinity towards Ni^{2+} ions. Then, one can speculate that the as-prepared adsorbent would exhibit an excellent reusability, as shown in Fig. 10. Clearly, by consecutive adsorption–desorption cycles, the adsorption capacities in the second and third cycle are found to be higher than that of initial one as a result of an increase in the adsorption sites during the regeneration process. Similar experimental phenomenon was also observed during the NH_4^+ adsorption by our earlier studies [23]. After the third adsorption–desorption cycle, the adsorption capacity for Ni^{2+} shows a little decrease as a result of the predominant occupancy of some adsorption sites by accumulative Ni^{2+} ions. Nevertheless, the adsorption capacity in the sixth cycle can reach 83% of the initial one, meaning its excellent reusability.

3.7. Adsorption mechanism

A careful study has been performed to compare the infrared spectra before and after the adsorption for Ni^{2+} (Fig. 11). The results indicate that after the adsorption, the asymmetric vibration absorption of carboxylate group has shifted from 1583 to lower wave number of 1561 cm^{-1}, while the symmetric vibration absorption of carboxylate group remains almost the same (1409–1408 cm^{-1}), which is arisen from the chelating interaction of carboxylate to Ni^{2+} ion. The formation of coordination bond of carboxylate with metals will diminish the charge density on the carboxylate oxygen and thus decrease the force constant of it [33]. In addition, the weaken absorption bands of reactive functional groups of CTS cannot be found after the adsorption for Ni^{2+}, indicating that these residual reactive functional groups are also involved in the adsorption process.

4. Conclusions

In this study, the recovery of a valuable metal Ni^{2+} was realized using CTS-*g*-PAA as the adsorbent. The as-prepared adsorbent shows good affinity to Ni^{2+} ion, with the maximum adsorption capacity of 161.80 mg g^{-1}. The adsorption equilibrium can be achieved within 30 min, and the as-prepared adsorbent can be applied in a wide pH range of 3–7. This adsorbent is observed to have good adsorption capacity for Ni^{2+} in the presence of Cu^{2+} and Pb^{2+}, and can be easily regenerated with no conspicuous losses in the adsorption capacity. Chelating interaction between the carboxylate groups and Ni^{2+} is the governing adsorption mechanism.

Acknowledgements

The authors thank the joint support by the National Natural Science Foundation of China (No. 20877077) and Science and Technology Support Project of Gansu Provincial Science and Technology Department (No. 0804GKCA03A).

References

[1] M.F.M. Bijmans, P.-J. Helvoort, S.A. Dar, M. Dopson, P.N.L. Lens, C.J.N. Buisman, Water Res. 43 (2009) 853–861.
[2] J. Kristiansen, J.M. Christensen, T. Henriksen, N.H. Nielsen, T. Menné, Anal. Chim. Acta 403 (2000) 265–272.
[3] E. Rudnik, M. Nikiel, Hydrometallurgy 89 (2007) 61–71.
[4] M.A. Rabah, F.E. Farghaly, M.A. Abd-El Motaleb, Waste Manage. 28 (2008) 1159–1167.
[5] P.G. Priya, C.A. Basha, V. Ramamurthi, S.N. Begum, J. Hazard. Mater. 163 (2009) 899–909.

[6] V. Sridhar, J.K. Verma, S.A. Kumar, Hydrometallurgy 99 (2009) 124–126.
[7] Z. Zainol, M.J. Nicol, Hydrometallurgy 96 (2009) 283–287.
[8] N. Jiang, X. Chang, H. Zheng, Q. He, Z. Hu, Anal. Chim. Acta 577 (2006) 225–231.
[9] S. Rastegarzadeh, N. Pourreza, A.R. Kiasat, H. Yahyavi, Microchim. Acta 170 (2010) 135–140.
[10] F. Marahel, M. Ghaedi, A. Shokrollahi, M. Montazerozohori, S. Davoodi, Chemosphere 74 (2009) 583–589.
[11] J. Seneviratne, J.A. Cox, Talanta 52 (2000) 801–806.
[12] K. Yamashiro, K. Miyoshi, R. Ishihara, D. Umeno, K. Saito, T. Sugo, S. Yamada, H. Fukunaga, M. Nagai, J. Chromatogr. A 1176 (2007) 37–42.
[13] T.P. Rao, S. Daniel, J.M. Gladis, Anal. Chem. 23 (2004) 28–35.
[14] Q. Wang, J.L. Mynar, M. Yoshida, E. Lee, M. Lee, K. Okuro, K. Kinbara, T. Aida, Nature 463 (2010) 339–343.
[15] X.-Z. Zhang, Y.-Y. Yang, T.-S. Chung, K.-X. Ma, Langmuir 17 (2001) 6094–6099.
[16] Q. Wang, X. Xie, X. Zhang, J. Zhang, A. Wang, Int. J. Biol. Macromol. 46 (2010) 356–362.
[17] A.T. Paulino, M.R. Guilherme, A.V. Reis, G.M. Campese, E.C. Muniz, J. Nozaki, J. Colloid Interface Sci. 301 (2006) 55–62.
[18] E.K. Yetimoğlu, M.V. Kahraman, G. Bayramoğlu, Ö. Ercan, N.K. Apohan, Radiat. Phys. Chem. 78 (2009) 1800–1806.
[19] Y. Zheng, J. Zhang, A. Wang, Chem. Eng. J. 155 (2009) 215–222.
[20] Y. Liu, Y. Zheng, A. Wang, J. Environ. Sci. 22 (2010) 486–493.
[21] S. Döker, S. Malcı, M. Doğan, B. Salih, Anal. Chim. Acta 553 (2005) 73–82.
[22] Y. Zheng, A. Wang, Chem. Eng. J. 162 (2010) 186–193.
[23] Y. Zheng, A. Wang, J. Hazard. Mater. 171 (2009) 671–677.
[24] V. Singh, A. Tiwari, D.N. Tripathi, R. Sanghi, Polymer 47 (2006) 254–260.
[25] R. Jayakumar, M. Prabaharan, R.L. Reis, J.F. Mano, Carbohydr. Polym. 62 (2005) 142–158.
[26] Y. Zheng, A. Wang, J. Macromol. Sci. A 47 (2009) 33–38.
[27] R. Donat, A. Akdogan, E. Erdem, H. Cetisli, J. Colloid Interface Sci. 286 (2005) 43–52.
[28] C.O. Ijagbemi, M.-H. Baek, D.-S. Kim, J. Hazard. Mater. 174 (2010) 746–755.
[29] M. Sprynskyy, B. Buszewski, A.P. Terzyk, J. Namiésnik, J. Colloid Interface Sci. 304 (2006) 21–28.
[30] R. Say, A. Tuncel, A. Denizli, J. Appl. Polym. Sci. 83 (2002) 2467–2473.
[31] A.T. Paulino, M.R. Guilherme, A.V. Reis, E.B. Tambourgi, J. Nozaki, E.C. Muniz, J. Hazard. Mater. 147 (2007) 139–147.
[32] M. Rao, A.V. Parwate, A.G. Bhole, Waste Manage. 22 (2002) 821–830.
[33] F. Huang, Y. Zheng, Y. Yang, J. Appl. Polym. Sci. 103 (2007) 351–357.